A consensus motif in *ASH1* and further transcripts unifies several RNA motifs required for interaction with the She2p/She3p transport machinery and mRNA localization in yeast

Markus Seiler[1#*], Annika Niedner[2#], Simone Heber[2,3], Michael Feldbrügge[4], Ralf-Peter Jansen[5], Dierk Niessing[2,3*], Kathi Zarnack[1*]

[1]Buchmann Institute for Molecular Life Sciences (BMLS), Goethe University Frankfurt, Max-von-Laue-Str. 15, 60438 Frankfurt a. M., Germany

[2]Institute of Structural Biology, Helmholtz Zentrum München, Ingolstädter Landstrasse. 1, 85764 Neuherberg, Germany

[3]Institute of Pharmaceutical Biotechnology, Ulm University, James Franck Ring N27, 89081 Ulm, Germany

[4]Institute of Microbiology, Heinrich-Heine University Düsseldorf, Universitätsstr. 1, 40225 Düsseldorf, Germany

[5]Interfaculty Institute of Biochemistry, Tübingen University, Auf der Morgenstelle 34, 72076 Tübingen, Germany

[#] Equal contribution

[*] Corresponding authors

Keywords: She2p, She3p, localization machinery, RNA localization, RNA zip-code, modeling, consensus motif, surface plasmon resonance, computational screening

Abstract

Asymmetric localization of the *ASH1* transcript is a central step in the regulation of mating type switching in *Saccharomyces cerevisae* and a paradigm for localized mRNAs specifically recognized by the She2p/3p transport machinery. Four RNA elements in *ASH1* are known to mediate bud localization, but it remained unclear what a consensus motif of all four She2p/3p recognition sites (SRS) might look like. In this study, we derive the SRS consensus motif, which is characterized by an L-shaped, double-stranded RNA conformation with two cytosine-containing sequence motifs at conserved positions and a central asymmetric bulge. It is noteworthy that the spatial arrangement of these features can be retained, despite their altered order within the nucleotide sequence. We termed these variations "configurations" and confirmed in biochemical studies that SRS function in *ASH1* elements is preserved when changing configurations. We tested other known and predicted SRS elements in target transcripts of She2p/3p by biochemical and biophysical studies and confirmed the conserved SRS function even in switched configuration. Consistently, we present the *SRS instance collection*, which includes further predictions of SRS instances of transcript targets of the She2p/3p translocation pathway.

42 **Introduction**

43 The active intracellular transport of effector molecules contributes to the high degree of
44 organization in life and asymmetric mRNA distribution is one way to ensure correct spatiotemporal
45 expression of encoded proteins [1]. In recent years, it has been studied in various polarized cells, in *D.*
46 *melanogaster* and *Xenopus laevis* oocytes and embryos [2–4], and also in mammalian fibroblasts [5] and neurons
47 [6]. mRNA transport is involved in embryonic patterning, cellular polarity, and asymmetric cell division.
48 Failure of mRNAs to be properly transferred has been shown to cause cellular dysfunction and disease [7]. In
49 these pathways, mRNAs are recognized by the cellular translocation machinery via *cis*-acting elements in
50 their sequences, called zip-codes or localization elements that may be determined by both, short RNA
51 sequence motifs, conformational folds [8–10] and spatial restraints between these features [11]. These zip-codes
52 are recognized by RNA-binding proteins that target the mRNAs to their final destination [12]. Within the
53 mRNAs, the zip-codes often reside in the 3' untranslated regions (3' UTRs) of mRNAs, but also in 5' UTRs
54 and coding regions [13–18].

55 Budding yeast (*S. cerevisiae*) has evolved as a model organism for mechanistic analyses on specific
56 targeting of mRNAs to the bud of emerging daughter cells [19,20]. The current model of how the RNA transport
57 machinery is built suggests a step-wise assembly of its core compounds: She2p interacts specifically with
58 its target mRNA and recruits the adapter protein She3p together with the type V myosin Myo4p [21–24]. This
59 mRNA ribonucleoprotein (mRNP) complex is then transported along the actin cytoskeleton. The paradigm,
60 the yeast *ASH1* mRNA, is localized to the bud tip enabling the asymmetric distribution of its encoded
61 transcription factor Ash1p into the daughter cell nucleus where it represses mating-type switching [25–28]. To
62 date, over twenty transcripts have been reported to be targeted via the She2p/3p machinery. Besides the
63 well-characterized She2p/3p target mRNAs *ASH1*, *EAR1*, and *WSC2*, further candidates were identified
64 using combined RNA immunoprecipitation and microarray techniques [24,29]. In some target mRNAs, the
65 regions containing putative zip-codes had been narrowed down by yeast three-hybrid and *in vivo*
66 localization studies [30]. However, besides of *ASH1*, precise positions of the She2p/3p recognition sites (SRS)
67 remained unknown in most cases. Within the *ASH1* mRNA, four localization elements with intrinsic SRS

68 function were mapped in accurate fashion [13,14,19]. Three of these (E1, E2A and E2B) were shown to reside
69 within the coding region, whereas E3 overlapped the stop codon and extended into the 3' UTR
70 (**Supplementary Fig. 1A, Tab. 1**). Each *ASH1* SRS element was sufficient for triggering the assembly of
71 the She2p/3p complex and for localizing a reporter RNA to the bud and was predicted to exhibit RNA folds
72 with extended stem-loop structures [13,14]. An *in-vivo* screen with mutated *ASH1* fragments supported the
73 notion that a three-dimensional fold was involved in zip-code function. The fold was described as a stem
74 with conserved nucleotides on either side: a singular cytosine and a CGA triplet, with a distance of six
75 nucleotides between the cytosines. Searching for similar RNA folds identified functional SRS elements in
76 *IST2* and *EAR1* [10]. However, these folds lacked an apparent consistency with some of the four *ASH1* SRS
77 elements and a coherent model for specific SRS recognition by the She2p/3p transport machinery has
78 remained elusive.

79 Recently, the interaction interface between E3 and She2p/3p was resolved using X-ray
80 crystallography: a symmetric tetramer of She2p exhibited two interfaces interacting with E3 on opposite
81 sides of the complex [8]. As suggested before [31], the affinity was increased by She3p in a synergistic manner.
82 Intriguingly, the ternary complex formation was accompanied by an induced fit in the SRS element: For
83 the unbound E3 RNA, SHAPE experiments suggested an elongated conformation [8]. When interacting with
84 She2p/3p, E3 displayed a sharp turn in one of its bulge regions, resulting in a kinked global conformation
85 that was also confirmed by NMR structures.

86 In this study, we define a coherent SRS consensus motif that unifies the features of E1, E2A, E2B
87 and E3 in *ASH1* and that also classifies SRS elements of further bud-localizing transcripts (*WSC2*, *EAR1,*
88 *IST2*). It exhibits a kinked stem-asymmetric bulge-stem-bulge structure, with the recurrent singular cytosine
89 in the asymmetric bulge and the CGA motif in a second bulge. One characteristic of the consensus motif is
90 its arrangement of features, conserved in the overall spatial arrangement but present in two variations
91 ("configurations") in linear sequences. Electrophoretic mobility shift assays and surface plasmon resonance
92 studies showed that E3 and other SRS elements could be switched between configurations without
93 impairing She2/3p binding. Using computational screening, we identified potential SRS instances in further

94 twelve transcripts known to interact with She2/3p. Finally, we introduce the *SRS instance collection*,
95 describing in detail predicted SRS elements and their positions in further RNA targets of the She2p/3p
96 translocation pathway.
97

98 **Results**

99 **Bioinformatics predictions reveal a consensus capturing all She2/3p recognition sites of *ASH1***

100 We wondered if a general concept may exist to describe all four localization elements of the *ASH1*
101 mRNA that act as She2p/3p recognition sites (SRS). For this study, we could rely on a recently published
102 crystal structure that showed in detail how the *ASH1* localization element E3 interacts in a kinked stem
103 structure with She2p/3p [8]. Of note, this interaction involved a molecularly induced fit upon binding that
104 resulted in an asymmetric bulge in the RNA stem with one of its functional cytosines deeply buried inside
105 the protein interface. We hypothesized that the ability to form such an asymmetric bulge could be a pre-
106 requisite of the E3 conformation, whose composition would require different lengths to be kinked. The
107 asymmetric bulge of E3 displayed a large stretch ("Lbulge") and a small one ("Sbulge"), with a length ratio
108 of 6 nt: 3 nt (**Fig. 1A**) (or 4 nt :1 nt, respectively, if considering atypical base pairing inside the bulge as
109 further base pairs). In a next step, we performed a systematic survey of such an arrangements in further
110 SRS elements of *ASH1*. However, common RNA conformation predictors do not consider precise structural
111 rearrangements due to RNA-protein interaction very well. In a step-wise strategy (**Supplementary Fig. 2,**
112 **Material and Methods),** we first evaluated which of the commonly used prediction tools would predict
113 the best approximation of the kinked E3 conformation in complex with She2p/She3p [8] just from the (single)
114 E3 nucleotide sequence. Of note, we found *Kinefold* [32] to predict the asymmetric bulge in close
115 approximation (5 nt : 2 nt) that could even be closer approximated if considering further details of the
116 crystal structure, resulting in (6 nt : 3 nt) (**Fig.1**, **Supplementary Fig. 3A**).

117 For E2A, we found the predicted conformation with an asymmetric bulge with exactly the same
118 length ratio as found in E3 (5 nt: 2 nt) using *Kinefold* (**Fig. 1B left)**. Surprisingly, after 180° rotation, the
119 arrangement of the predicted E2A conformation harmonized perfectly with the E3 conformation (**Fig. 1A**
120 **right, 1B right**). Furthermore, this 180° rotation caused the previously diverging sequence motifs of E3 to
121 fit now to the single and triplet motifs of E2A. Sequence comparison revealed 89% sequence identity
122 between E3 and E2A in the asymmetric bulge and flanking regions (**Supplementary Fig. 1B**). For E1, the

123 180° rotation of its predicted conformation resulted in an arrangement comparable with E3 (**Fig. 1D**), but
124 with different length proportions of the asymmetric bulge and a lower degree of sequence identity.
125 These findings suggested one blueprint, with a common overall spatial arrangement of its
126 (conformational and sequence) features in E3, E2A and E1 that we referred to as "SRS consensus motif"
127 (**Fig. 1E,F**). Of note, despite of this conserved spatial arrangement of features, their linear order was
128 interchangeable in the nucleotide sequences (**Fig. 1F**). This was due to the fact that we had to harmonize
129 conformations of E3, E2A and E1 by a 180 degree rotational step of E3. Subsequently, the 5' start of E3 is
130 at the opposite site of the SRS consensus motif than for E2A and E1, resulting again in different feature
131 orders in the nuclear sequence (**Fig. 1E**). We termed these variations "configurations", with "config-I"
132 observed in E3 and "config-II" in E2A and E1. In a next step, we refined the annotation of sequence motifs
133 in E3. We referred to the single cytosine motif in the asymmetric bulge as C_1 and to the cytosine in the
134 CGA motif as C_2 (**Fig. 1A, right, 1E**), analogously to E2A and E1. At first glance, the conformational
135 prediction of E2B displayed the hypothesized "Lbulge" even shorter than the "Sbulge" (**Fig. 1C, left**).
136 Remarkably, Kinefold predicted an alternative conformation with an asymmetric bulge in agreement with
137 the SRS consensus motif (6 nt: 3 nt), but with a 30% higher content of energy (calculated free energy = -
138 10.3 kcal/mol versus -7.4 kcal/mol), which could be rearranged by sliding the sequence repeats of the SRS
139 element (**Fig. 1C, right**). Altogether, we had derived a model of the SRS consensus motif (see **Info-Box**).
140 In a subsequent step, we could confirm that the model was sufficient to summarize previous functional
141 studies with mutationally-derived decreases in RNA localization in all four *ASH1* SRS elements [10,13,14,25]
142 (**Material and Methods)**. For a better overview, the distinct modeling steps (initially characterized
143 elements, Kinefold prediction, rotation, and mutual feature alignments) are displayed in (**Fig. 2**).
144
145 **The two configurations are interchangeable in E3 without loss-of-function *in-vitro***
146 One unexpected characteristic of the SRS consensus motif was the spatial conservation of its
147 features in its overall conformation while the order of features in the nucleotide sequences was found to be
148 swapped for the different configurations. To validate if we had grasped the essence of the consensus, we

149 investigated if an artificial switch between the different sequence orders (and the configurations) would
150 conserve SRS function. For this purpose, we used the well-characterized construct $E3_{51nt}$wt [8] and switched
151 its feature order in the nucleotide sequence (config-I) to design a config-II construct ($E3_{51nt}$switch, **Fig. 3A**).
152 Based on the observation that the E3 crystal structure exhibited an interaction of She2p/3p with C_2G but
153 not with C_2GA, and for comparability reasons with previous studies, we limited the construct design to
154 C_2G. Using an electrophoretic mobility shift assay (EMSA), we examined $E3_{51nt}$switch for interaction with
155 She2p and She3p in a titration approach. We used the fusion protein She2p-She3p, which comprised both,
156 She2p and a She3p fragment and was demonstrated to be sufficient to mediate the synergistic binding of
157 both proteins [8]. For the wildtype construct $E3_{51nt}$wt, we observed an interaction strength at the expected
158 nanomolar protein concentration (**Fig. 3A**) [8]. As a control, we tested the construct $E3_{51nt}$M6 characterized
159 by reduced interaction due to a $C_{1813}G$ substitution of C_2 [8]. In agreement of our model, $E3_{51nt}$wt and
160 $E3_{51nt}$switch, interacted with She2p-She3p at comparable nanomolar protein concentration (**Fig. 3A**). These
161 similar binding affinities contrasted with $E3_{51nt}$M6, which displayed severely impaired interaction.

162 Since the $E3_{51nt}$M6 mutant showed impaired but still considerable binding to She2p-She3p-fusion
163 protein, we used the full-length proteins to assess the binding features of E3 elements. Incubation with
164 constant She3p concentration of 0.56 µM and titration of She2p (0.02 - 5 µM) confirmed that both
165 constructs, $E3_{51nt}$wt and $E3_{51nt}$switch, supported binding even at the lowest She2p concentration used in this
166 experiment (0.02 µM). In contrast, binding of the full-length proteins to $E3_{51nt}$M6 was abolished at
167 concentrations up to 5 µM (**Supplementary Fig. 4B**) x. The same was true for a reciprocal approach, in
168 which increasing concentrations of She3p (0.02 - 5 µM) were tested in the presence of high amounts of
169 She2p (5 µM) (**Supplementary Fig. 4C**). Moreover, both experiments showed that She3p efficiently binds
170 E3 in the absence of She2p. Surprisingly, this binding was sensitive to mutation of C_2. In conclusion, these
171 studies successfully confirmed that E3 can be switched from config-I to config-II without compromising
172 its functionality to interact with She2p/3p.

173 When we analogously examined E2A and E1, we reversed the direction of switching (now from
174 config-II to config-I), resulting in the constructs $E1_{27nt}$switch and $E2A_{32nt}$switch (**Supplementary Fig. 5**).

175 Again, in EMSA validations, we could demonstrate that both constructs largely exhibited the binding
176 properties to She2p-She3p-fusion. In summary, the "config-switch" approach supported our model, which
177 suggested that SRS features could be rearranged in the RNA sequence while retaining function. We could
178 demonstrate that E1, E2A, and E3 recognized She2p/3p regardless of configuration, demonstrating the
179 essential characteristics of RNA-She2p/3p recognition were reflected in the SRS consensus motif. As a
180 conclusion, these findings indicate that SRS function requires very few conserved bases in defined positions
181 of a stem-loop, which must accommodate a bulge that is flexible enough to open up upon binding by She2p-
182 She3p to adopt a kinked L-shaped conformation in the co-complex.

183 In a fine-grained approach, we used the analytical power of surface plasmon resonance (SPR), to
184 investigate the influence of the functional cytosines C_1 and C_2 on SRS function. Previous studies had
185 determined a preferred distance of six nucleotides between these cytosines [10]. Using the functionally
186 minimal construct $E3_{29nt}$ [8], we introduced varying distances between C_1 and C_2 and performed titration
187 series in a surface plasmon resonance experiment with a She2p-She3p-fusion construct (125 nM) (**Fig. 3B**).
188 As a result, for the wildtype construct $E3_{29nt}$wt, we observed a binding affinity of approx. K_D = 0.89 nM
189 (**Fig. 3B, Supplementary Fig. 6**). In contrast, constructs with C_1-C_2 distances of five and seven nucleotides
190 led to a reduction in binding of at least one order of magnitude (**Fig. 3B**, **Supplementary Tab. 1**),
191 confirming the findings of 6 nt as optimal C_1-C_2 distance.
192

193 **A computational algorithm to screen for the consensus in known She2p/3p substrates**

194 We performed computational screening (details, see **Material and Methods**) to identify further
195 instances of the SRS consensus motif in further target sequences of the She2p/3p transport machinery. For
196 this purpose, we screened a list of 24 transcripts reported to show *in-vitro* binding by She2p/3p or bud
197 localization *in-vivo* [24,29,30]. The identified sequence regions represented potential SRS instances and were
198 evaluated for their potential to form the correct conformation of one of the configurations, again using
199 *Kinefold* for this step We intended to extend this conformational evaluation by integrating data describing
200 the degree of unpaired state of nucleotides (obtained in a remarkable genome-wide study using parallel

201 analysis of RNA structure (PARS), [33]). This strategy was promising, but for our purposes the data were not
202 detailed enough, as the averaged values for each nucleotide position suggested competing RNA
203 conformations even for some of the strong *ASH1* SRS elements (**Material and Methods, Supplemental**
204 **Fig. 7**).

205 For the three transcripts *EAR1, IST2* and *WSC2*, their SRS elements had been identified already,
206 with their sequence regions narrowed down to fragments [10,30]. Now, with knowledge of the SRS consensus
207 motif, these SRS elements could be classified as a config II arrangement (**Fig. 4C, Supplementary Fig. 8**).
208 Remarkably, for *EAR1* and *IST2*, the asymmetric bulge was even more eccentric than observed in *ASH1*
209 (*EAR1:* 7 nt :0 nt; *IST2*: 9 nt : 1 nt). In addition, we identified an additional upstream SRS instance in each
210 transcript, *EAR1* and *IST2* (**Tab. 2**). In contrast, for *WCS2*-C, the initially identified SRS fragment turned
211 out to comprise possibly two SRS elements, a canonical one in the center of this fragment, and a potential
212 SRS instance in the flanking regions, however, with a C_1-C_2 distance of 7 nt (**Supplemental Fig. 8D**).
213 However, we could not classify the second published instance in *WSC2*, *WSC2*-N, in agreement with our
214 model (see **Discussion**). As a first outcome of the screening we had identified seven SRS instances (**Fig.**
215 **3C**). When we studied the seven canonical SRS elements in detail, we noticed a recurring di-adenosine in
216 the L-bulge ("AA_L") as a common feature in all elements (**Fig. 3C**), possibly indicating relevance in SRS
217 function. This was surprising due to the fact that the crystal structure of E3 showed the interaction between
218 She2p/3p and the AA_L nucleotides occurs exclusively via the backbone atoms of the nucleotides, and thus
219 unspecifically [8], with their nucleobases having intramolecular contact within the RNA structure. This
220 observation makes relevance in the context of SRS recognition less likely. As mentioned before, for most
221 known SRS instances (20 of 24 instances in our set), functionality had been exclusively studied for large
222 RNA fragments or complete transcripts. For 13 of these transcripts, we could identify now the positions of
223 SRS instances. For 12 transcripts, we found one or two instances in each sequence, and we found four
224 instances in *TPO1* (**Fig. 4A**). Altogether, in 17 of 24 sequences (*ASH1*, *WSC2*, *EAR1*, *IST2* included), we
225 predicted 31 SRS instances, with ten instances (32%) in config-I and 21 instances (68%) in config-II,

226 respectively (**Fig. 4A**). Of notice, almost two thirds of the SRS instances contained the AA_L di-nucleotide
227 in the Lbulge (**Fig. 4B)**.
228
229 **Validation of SRS elements in *EAR1*, *IST2*, *KSS1* and *TCB3***
230 As described before, in *IST2* and *EAR1*, sequence fragments with SRS function had been identified
231 already, and these sequences were also identified in our computational screening (termed *EAR1*-SRS2,
232 *IST2*-SRS2; referring to the nomenclature, see **Tab. 2**). We could classify their functional features, in
233 agreement with the SRS consensus motif, provided that the consensus was valid also for all these instances.
234 In such a view, the SRS elements would resemble the very first characterization (Olivier et al., 2005),
235 however in the larger context of a SRS consensus motif. To address this aspect, we studied the interaction
236 between specifically designed SRS constructs and She2p-She3p fusion proteins, analogous to our previous
237 studies. In accordance with the consensus, the newly designed constructs $EAR1_{26nt}$switch and $IST2_{29nt}$switch
238 were strictly reduced to those regions assumed to be essential for SRS function and also switched in
239 configuration (each to config-I) (**Fig. 5A**). As we could show in EMSA studies, $EAR1_{26nt}$switch was bound
240 with affinities comparable to the unmodified wild-type element $EAR1_{50nt}$wt (**Fig. 5A**). Although for
241 $IST2_{29nt}$switch binding was clearly retained, it was considerably weaker when compared to $IST2_{62nt}$wt. In
242 addition, the *SRS instance collection* contained instances in transcripts for which no detailed position
243 information on SRS instances in transcripts had previously been determined. From these instances, we
244 chose *KSS1*-SRS1 (config-II, **Tab. 2**) and *TCB3*-SRS1 (config-I, **Tab.2**) for further functional analysis. As
245 a result, we were able to show that $KSS1_{72nt}$wt interacts strongly with the She2p/3p fusion protein *in-vitro*
246 (**Fig. 5B**) and observed similar strong binding for the minimal construct switched in configuration
247 $KSS1_{29nt}$switch (to config-I), confirming *KSS1*-SRS1 as a potential SRS element. In an analogous manner,
248 we tested the minimal construct $TCB3_{38nt}$wt (config-I) and observed also strong interaction with the fusion
249 protein (**Fig. 5B**) confirming also *TCB3*-SRS1 as potential SRS element. In summary, we were able to
250 demonstrate the identification and *in-vitro* confirmation of new SRS instances. Furthermore, for some of
251 these instances we were able to prove that the newly designed, size-reduced constructs retain the SRS

252 function even in switched configuration. In conclusion, the fact that our model, derived exclusively from
253 *ASH1* SRS elements, enabled the identification, size reduction, and config-switch of designed SRS
254 constructs in previously unexplored sequences while preserving SRS function confirmed its applicability
255 as an SRS consensus motif.
256
257 **Validation of further features in the SRS of *EAR1***
258 In *EAR1* (*YMR171C*), it had been shown for its SRS element (now termed *EAR1*-SRS2) that
259 substitutions in the sequence motifs decreased function [10]. The substitution of both, C_1 (updated
260 nomenclature) (construct "M2" in [10]) and C_2 (construct "M1") had shown severe effects *in-vivo*. To examine
261 the SRS consensus motif and *EAR1*-SRS2 in more detail, we chose a fine-grained approach using the
262 $EAR1_{31nt}$switch construct (switch to config-II) as the base construct for further changes (**Fig. 6A**) and
263 determined its binding affinity using SPR analysis as described before. As result, we obtained an affinity
264 of the original construct $EAR1_{31nt}$switch of K_D = 11 nM (**Fig. 6D, Supplementary Fig. 9**). Remarkably,
265 compared to the E3 minimal element, the affinity with the She2p/3p fusion protein was decreased by one
266 order of magnitude ($E3_{29nt}$wt: K_D = 0.89 nM). When we examined the original construct $EAR1_{31nt}$switch for
267 modifications in the inverted repeat IR1, by inversions or additionally introduced base pairs, the modified
268 constructs showed affinities in the range of the original construct suggesting no direct impact on SRS
269 function (**Fig. 6D**). Second, we examined the function of the di-nucleotide AA_L in the Lbulge by deletions
270 of varying extent (**Fig. 6C**), analogously observing binding affinities in the magnitude of the basic construct
271 (**Fig. 6D**). The analysis of the functional cytosines C_1 and C_2 was complex since two cytosines (C_{1601} and
272 C_{1602}) precluded an unambiguous assignment of the C_1 position (**Fig. 6B**). The substitution of either cytosine
273 (constructs $C_{1\text{-}1}$U, $C_{1\text{-}2}$U) resulted in a considerable binding decrease suggesting that both positions
274 contribute to She2p/3p binding (**Fig. 6D**). Unexpectedly, a deletion of one of the C_1 positions (ΔC_1) or a
275 simultaneous substitution of both cytosines ($C_{1\text{-}1}$ U & $C_{1\text{-}2}$ U) restored She2p/3p binding (see **Discussion**).
276 In contrast, substituting C_{1590} in the three-nucleotide C_{1590}GA motif (C_2U) returned unequivocal results
277 manifesting in a dramatic loss of binding. Altogether, these results confirmed that neither sequence

278 composition of IR1 nor the AA_L motif in the Lbulge were relevant for She2p/3p binding *in vitro*. Alterations
279 of the C_1-C_2 distance were tolerated in some SRS contexts but not others, with a strong bias for a C_1-C_2
280 distance of six nucleotides. We therefore kept a C_1-C_2 distance constraint of six nucleotides for subsequent
281 computational SRS screening.
282
283 **A collection of predicted *SRS* instances in known target transcripts of She2p/3p**
284 Computational screening for the SRS consensus motif had identified SRS instances in 17 of 24
285 sequences (**Fig. 4A**). After positive *in-vitro* validation of several of the new SRS instances (in *EAR1*, *IST2*,
286 *KSS1*, *TCB3*), we finally created a collection of these screening results to present to the community (*SRS*
287 *instance collection*, **Tab. 2**). This collection contains information on 32 SRS instances in 17 transcripts that
288 have been reported to show She2p/3p binding *in-vitro* or bud localization *in-vivo* [24,29,30]. In addition, a
289 standardized nomenclature for SRS elements is introduced and further information is provided on positional
290 data, classification and other details of SRS instances, several of them are promising new candidates for
291 future experimental investigations.

292 **Discussion**

293 In this work, we have derived the unified model of a three-dimensional RNA motif that functions
294 as She2p/3p recognition motif (SRS) with the She2p/She3p protein transport machinery, a prerequisite for
295 active transport of transcripts to the yeast bud. We used a computer-aided and conceptual modeling
296 approach that based on the hypothesis that an asymmetric bulge in the RNA conformation might be a
297 prerequisite of SRS function. This approach led to the identification of a common three-dimensional
298 arrangement of SRS functional features (conformational features and sequence motifs) in the *ASH1*
299 localization elements E3, E2A and E1 (and with limitations also for E2B) in a blueprint, thus demonstrating
300 the long-missing consensus motif of all four SRS elements. Unexpectedly, although this arrangement of
301 features was conserved in its overall three-dimensional fold, , there were two variations with respect to the
302 linear arrangement in the nucleotide sequences. We termed these variations "configurations" ("config-I" in
303 E3, "config-II" in E2A, E1 and E2B). The consensus model proved to be correct based on our consistent
304 results from electric mobility shift assays, in which we analyzed the SRS function of RNA-constructs with
305 re-designed feature arrangement. According to our model, this rearrangement of the features affected their
306 linear order in the nucleotide sequences, but allowed the preservation of their overall three-dimensional
307 arrangement. This re-design therefore represents a switch between their original configuration and the
308 respective counterpart configuration ("config-switch"). We were able to consistently demonstrate that the
309 config-switch retained SRS function in all experiments we performed indicating that the consensus motif
310 comprises the main requirements of SRS function. The fact that also size-reduced constructs proved to keep
311 SRS function was a further hint that we had grasped the essential features of SRS function. It can be
312 described in all *ASH1* SRS elements as follows: an asymmetric bulge, flanked by inverted repeats, forms a
313 kinked, L-shaped RNA conformation. The larger side of the bulge contains the single cytosine motif C_1
314 inside of the first three positions. The C_2GA motif resides on the opposite strand of C_1, separated by an
315 inverted repeat in downstream direction on this strand. The two configurations are marked by the two
316 different 5' entry sites into this kinked conformation. These findings were further confirmed, when we
317 compared previous thorough mutagenesis studies of the *ASH1* SRS elements and could assign these results

318 well according to their relevance in the SRS consensus model. Further, by studying the binding kinetics of
319 $E3_{29nt}$wt in surface plasmon resonance analysis, we could confirm the optimal distance between C_1 and C_2
320 with six nucleotides as it was suggested before (ca. 28 Å) [10]. It is noteworthy that the existence of two
321 (double-stranded) configurations that can be converted into each other by swapping their features in the
322 nucleotide sequence finds an analogy in studies on the beta-actin RNA zip code, where the order of its
323 (single-stranded) 5' and 3' elements is interchangeable within the target transcripts bound to ZBP1 [11].

324 Due to its universal character to describe all four *ASH1* SRS elements, the exploitation of the SRS
325 consensus motif went beyond previously proposed computational screening strategies. Hence, we created
326 a computational screen that searched for both configurations, followed by a conformational check of the
327 overall RNA fold performed by *Kinefold*. For some of the further transcripts that had been found to localize
328 at the bud tip of yeast cells, sequence fragments had already been narrowed down with retained SRS
329 function. In this set of sequence fragments, we could classify SRS elements of *EAR1*, *IST2* and *WSC2* as
330 further instances of the SRS consensus motif.

331 *EAR1* was first identified as localized in the bud by [29] with its SRS element characterized in further
332 studies [10] and classified as a config-II SRS element in this work (*EAR1*-SRS2, **Tab.1**). We were able to
333 confirm previous studies that the specific nucleotide sequences of the inverted repeats did not contribute to
334 SRS function [8,13]) by applying SRP to different modifications of the minimal construct $EAR1_{31nt}$switch. In
335 contrast, the loss of C_2 showed a strong impact on SRS function that was also consistent with previous *in-*
336 *vivo* studies [10]. Analogously, individual substitutions of each of the two potential C_1 positions (in C_1-C_2-
337 distance of five or six nucleotides) affected SRS function. Unexpectedly, a single deletion of C_{1601} or a
338 simultaneous substitution of C_{1601} and C_{1602}, both restored SRS function. When studying the potential di-
339 nucleotide AA_L sequence motif by deletion experiments we could not detect any direct impact on SRS
340 function, even if the Lbulge region was almost completely deleted. So far, we can neither explain the
341 apparent discrepancy in the C_1 mutation effects in the *EAR1* constructs nor the retained SRS function with
342 deleted asymmetric bulge. It may reflect both complex sequence composition and inherent redundancy in
343 this particular SRS instance.

344 So far, we had observed a config-I arrangement only in E3 whereas we had identified six SRS
345 elements with config-II (**Fig. 4C**). This dominance of config-II SRS elements continued when we applied
346 the computational screen to our complete sequence set and predicted 31 instances in 17 sequences, with 22
347 predicted elements (71%) exhibited config-II. So far, the reason for the unequal frequency of the two
348 configurations remains unclear. For each of the two sets of SRS instances (with relatively well-known
349 positions in their transcripts or with unknown SRS positions), we experimentally analyzed two instances,
350 utilizing EMSA approaches as described before. For the first subset, we could confirm SRS function of
351 previous studies in both SRS elements *EAR1*-SRS2 and *IST2*-SRS2 [10]. For the second subset, we could
352 verify both new identified SRS elements *KSS1*-SRS1 and *TCB3*-SRS1 *in-vitro.* Remarkably, when we
353 switched configuration in *EAR1*-SRS2, *IST2*-SRS2 and *KSS1*-SRS1 (config-II to config-I), we could
354 demonstrate again conserved SRS function for <u>all</u> switches, strongly supporting the SRS consensus model.
355 Of note, as a first successful validation *in-vivo*, we had been able to identify and confirm the nucleotide
356 positions of a SRS element in the *CLB2* transcript [34]: In the transcript, only a few but functionally crucial
357 positions of the SRS instance *CLB2*-SRS1 (config-II, 1111 nt - 1145 nt) were altered in non-canonical
358 mutations to reveal a significant loss-of-function effect in bud-localization and a shift in protein distribution
359 from the buds towards mother cells. It is also interesting to note that the regulatory effect of well-defined
360 asymmetric bulges seems not to be limited to SRS function. As described in [35], the structure of the pre-
361 mRNA autoregulatory complex of the L30 ribosomal protein in yeast displays an asymmetric bulge (length-
362 ratio 5 nt : 2 nt) with a cytosine positioned in an extension of the Lbulge, and separated from another
363 cytosine (in a further bulge) by an IR in a distance of 6 nt. Remarkably, it is this asymmetric bulge region
364 that is part of a mutual induced fit, suggesting analogies with the observed induced fit mechanisms in the
365 crystal structure of E3 and She2p/3p.

366 Further aspects of SRS characteristics remain to be investigated. For example, a further extension
367 of the description of the SRS consensus motif is thinkable: It is reasonable to ask if the SRS function would
368 be conserved if Lbulge and Sbulge were joined together without IR2 as intervening feature. Although
369 experimental analysis of such a setting is beyond the scope of this study, we would like to put to discussion

370 such a theoretical construct, to possibly take a step forward to complete the picture (**Supplementary Fig.**
371 **10A**). The SRS element *WSC2*-N [36] that could be not classified, might be such an example (**Supplementary**
372 **Figure 10B, left**). Such an extended perspective might have further implications also for the understanding
373 of some of the SRP results of *EAR1* described before. Both elements, *EAR1*-SRS2 and *IST2*-SRS2 displayed
374 two CGA motifs with the following consequences: Whereas we considered *EAR1*-SRS2 as config-II with
375 C_2GA residing in the terminal bulge, this terminal bulge also may be considered as a joint of Lbulge and
376 Sbulge, hence offering a new perspective: the cytosine motif in this terminal bulge may be considered as
377 C_1 while its counterpart (initially referred to as C_1 inside of the asymmetric bulge) may be extended to
378 C_2GA (**Supplementary Figure 10B, right**). In such a view, the functionality of *EAR1*-SRS2 would exhibit
379 redundant features of two superimposed and oppositely rotated SRS elements in the bigger context of an
380 (extended) consensus motif. This perspective may also explain partially the ambiguous results in the SPR
381 experiments of our study. Secondly, a further extension of the SRS consensus could be formed by a range
382 in the C_1-C_2 distance. In consistency with previous studies [10] and with our SPR results we focused on the
383 optimal parameters of six nucleotides in this study to minimize false positive matches. However, we could
384 not exclude a minimal functionality for instances with (C_1-C_2 distance $\neq 6$). An example might be a second,
385 potential SRS instance that we identified in the flanking regions of *WSC2*-SRS2 (*WSC2*-C) but with a C_1-
386 C_2 distance of seven nucleotides (**Supplementary Fig 7C**). In such a case, *WSC2*-SRS2 may compensate
387 the suboptimal C_1-C_2 distance of its neighboring SRS element by inducing SRS conformation in a
388 cooperative manner when both SRS instances interact with the binding interfaces on the opposite sites of
389 the She2p tetramer [37].

390 As a second aspect, localization elements that mediate bud localization require the interaction with
391 the She2p/3p protein transport machinery, but further motifs may be required as binding platforms of
392 auxiliary factors. For E2B, we have speculated that its energetically optimized conformation had to be
393 rearranged from an alternative conformation to display the SRS consensus motif. Even strong SRS elements
394 such as E2A [12] can be subject to major reorganizations, as shown by the PARS data which indicate
395 competing conformations for E2A [33] (**Supplementary Fig. 7**). Therefore, the She2p/3p interaction can be

seen as a central step in the zip-code function, but it might be framed by further rearrangements in the chronological order. In such a scenario, transient binding of auxiliary cofactors could stabilize the asymmetric bulge and increase SRS function. AA_L might be such a co-factor binding motif. Despite the fact that AA_L was present in each case of our seven well-characterized, bud-localizing SRS elements, neither the crystal structure of [8] nor the results of SPR studies suggest involvement in She2p/3p binding specificity. Future research must clarify the possible function of AA_L *in-vivo*, also with regard to transient interactions. In addition, for E3 and E2A, it was tempting to speculate if their extraordinary sequence identity was a product of convergent evolution, due to further requirements in affecting zip-code function. Maybe we have to face a trade-off between canonical SRS consensus motif and stability of the individual RNA conformation, with the weakening of one aspect may be compensated by strengthening of the other. This would complicate the identification of SRS instances, especially if auxiliary co-factors would alter the probabilities of formation of SRS conformations *in-vivo*. Summarizing, all these aspects stress two aspects: (i) The new SRS consensus motif delivers a conceptual framework of how to classify further aspects of new SRS instances, and (ii) It remains necessary to combine experimental screenings (identification of bud-localizing transcripts, final validation of instances) and computational screenings (prediction of positional information in transcripts to narrow down experimental analysis and suggest crucial positions in mutations studies). Consequently, the *SRS instance collection* contains only such SRS instances where bud localization had been confirmed already, at least at the transcript level.

In conclusion, the SRS consensus motif enabled the description of the four SRS elements of *ASH1* in one model, hence providing the long-missing consensus. It further unified the described functional features of the known SRS elements in *IST2*, *EAR1* and *WSC2* and enabled the identification of new SRS elements in further bud-localizing transcripts. The consensus model proved to be consistent with previous mutagenesis studies of these elements and we could demonstrate that a switch between the configurations retained function in SRS constructs of several transcripts.

420 **Materials and Methods**

421 **Overview on the theoretical data flow to derive the SRS consensus model**

422 The theoretical part of deriving the SRS consensus model comprised the following steps
423 (**Supplementary Fig. 2)**: (1) Hypothesis (asymmetric bulge as hallmark of SRS) by analysis of crystal
424 structure of *ASH1*-E3 (2) Selection of an appropriate conformational prediction tool (3) Conformational
425 prediction of instances and inspection to derive a consensus (**Fig. 2**) (4) Cross-check of the consensus with
426 published functional data (5) Creation of a computational screening pipeline (6) Check for further data
427 sources to filter results (**Supplementary Fig. 7**) (7) Screening for instances in selected sequence sets (8)
428 Inspection of instances for further patterns

429

430 **Identification of an appropriate conformational prediction tool**

431 The inspection of the crystal structure of *ASH1*-E3 suggested an asymmetric bulge as a pre-requisite
432 of kinked RNA conformation. The occurrence of such asymmetric bulges may be favorized in mRNPs by
433 the energy release due to molecular interaction. However, its occurrence is less likely in an individual RNA
434 and is less likely to be predicted as plausible conformation by computational prediction tools that commonly
435 deal with individual RNA sequences. In a survey, when investigating which of common tools [32,38–40] was
436 most likely to predict the asymmetric bulge of E3, we found Kinefold [32] as the one that best tolerated
437 asymmetric bulges (**Supplementary Fig. 3**). It predicted the asymmetric bulge consisting of a 5 nt Lbulge
438 and a 2 nt Sbulge, which closely approximates the length ratio of the asymmetric bulge observed in the E3-
439 She2p/3p crystal structure [8] that displayed a length ratio of 6 nt : 3 nt (considering only Watson-Crick base
440 pairs) or 4 nt : 1 nt (considering also non-canonical base pairings as found in the crystal structure),
441 respectively (**Fig. 1A**).

442

443 **Cross-check of the consensus with published functional data**

444 We used published data of functional studies that involved both, mutagenesis and deletion of RNA
445 regions to cross-check for consistency with the SRS consensus model [10,13,25,30]. We characterized such

446 mutations in *ASH1* SRS elements that could clearly be assigned to destroy or to keep SRS function
447 according to the consensus model. All these constructs were in accordance with the consensus model (data
448 not shown).
449
450 **Development of a computational screening approach**
451 For the purpose of identifying further instances of the SRS consensus motif, we transformed the
452 consensus features into "patterns" to screen for "matches" in RNA sequences. We created a computational
453 screening pipeline consisting of in-house computational scripts and an external conformational prediction
454 algorithm. For the screening, three aspects were required: (1) Screening the sequence for conformational
455 aspects. For each RNA, the sequence was screened for two nested pairs of inverted repeats (each with a
456 minimal length of four nucleotides) that framed an asymmetric bulge region. We had to consider both
457 configurations in different screening patterns. The obtained constituted potential SRS instances. (2)
458 Screening the sequence for functional motifs. For each SRS instance, the Lbulge region was screened for
459 C_1, the opposite strand for C_2GA (positioned beyond IR1), with a C_1-C_2 distance of 6 nt between. The
460 screening strategy based on the approach of modular feature screening of mosaic-like patterns [41]. This
461 modular approach allowed to introduce further features to be screened (e.g., AA_L). It also tolerated length
462 variations between the distinct (sequence and conformational) features (e.g., one version tolerated C_1
463 positioned in the last nucleotide of IR1). As a consequence, permutated sets of varying patterns could be
464 summarized into two screening patterns (one for each configuration). (3) Validation by conformational
465 prediction. For each SRS instance, it was calculated if it would express a stable conformational fold that
466 fitted to the conformational arrangement of the SRS consensus. This analysis was performed using *Kinefold*
467 as energy-minimization approach that had proven best for large asymmetric bulges. On each site , the SRS
468 stretches were extended by 10 nt of the flanking sequences of their RNA sequences, to tolerate some degree
469 of freedom during calculation. In a series of tests using known SRS elements, a flanking region extension
470 by 10 nt had proven to be best in a range of 0 nt to 50 nt (data not shown). Of note, natural limitations of
471 common RNA conformational predictions occur due to the fact that such calculations are limited to predict

472 the conformation of distinct RNA stretches but less reliable regarding statements of the complete transcript
473 and second, they would ignore any energetic benefits by binding of molecular interactors (e.g., She2p/3p
474 proteins). As a consequence, we analyzed the 25th best conformational predictions of *Kinefold* (maximum
475 value = 25), to consider slight structural dynamics in each RNA molecule.
476
477 **Check for further data sources to filter for the consensus**
478 For the purpose to possibly extend the validation step of new SRS instances by conformational
479 predictions. we intended to cross-check the predicted conformations with experimental data to get deeper
480 insights on actual RNA conformations *in-vivo*. For our purposes, we tested the remarkable genome-wide
481 study based on PARS (Parallel Analysis of RNA Structure) [33]. For each nucleotide in transcripts, PARS-
482 scores described the percentage in occurring in single-strand ("S1-reads" of RNase S1) or double-strand
483 ("V1-reads" of RNase V1) regions of the RNA conformations. We extracted the S1- and V1-data and tested
484 the strong localization element E3 [13] as positive control. As a result the PARS data was well suited to
485 describe the SRS conformation as observed in the E3 crystal structure [8] (**Supplemental Fig. 7**). However,
486 for further controls, the data comparison of paired/ unpaired occurrence of nucleotides between PARS data
487 and SRS consensus model failed (**Supplemental Fig. 7**). Commonly, RNA molecules display not one
488 distinct conformation in-vivo but are subject to conformational dynamics resulting in collections of
489 competing conformations. PARS data per nucleotide averaged the binding state (paired/unpaired) over all
490 competing conformations. It seemed that even the two SRS elements in *ASH1*-E1 and *ASH1*-E2A that were
491 shown to function as efficient localization elements [13] were not so stable in their consensus conformations
492 that these would be so conspicuous that they could be distinguished from alternative conformations in the
493 PARS data.
494
495 **Further bioinformatics resources**
496 For the investigation of molecular structures, we used Pymol [42] as 3D- viewer. Initial protein
497 characterization of She2p and She3p was performed using the ELM server [43]. RNA sequence alignments

498 were performed using Jalview [44]. RNA sequences were extracted of the Saccharomyces Genome Database
499 [45]. For the actual screening, the mRNA sequences of *ASH1*, *IST2*, *EAR1* (aka *YMR171C*), *WSC2* and 20
500 further mRNA sequences known to She2p/3p interact [10,13,25,29,30,36] (Chartrand1999; Chartrand2002;
501 Olivier2005; Takizawa2000; Shepard2003; Jambhekar2005) were chosen. As sequence data, we used the
502 CDRs, extended by 200 nt downstream by default, due to the fact that for several mRNAs, the actual 3'UTR
503 lengths were still unknown. Functional annotation of Supplementary Table S1 followed [46]. Graphical
504 visualization of RNA conformations was performed using VARNA [47].
505
506 **Protein expression**
507 Expression in *E. coli* and purification of She2p, She3p, their fusion protein, and variants thereof
508 were performed as described in [8,23]. Purity and solubility were confirmed by size-exclusion chromatography
509 and SDS page.
510
511 **RNA preparation and isotope labeling**
512 For small scale *in vitro* transcription the MEGAshortscript T7 kit (life technologies) was used
513 according to the manufacturer's instructions. Synthetic DNA oligonucleotides containing a T7 promoter
514 and the respective sequence were used as a template. After *in vitro* transcription, the template was digested
515 by DNAse and the RNA was extracted using phenol:chloroform:isoamyl alcohol (25:24:1). Homogeneity
516 of RNA was assessed by native and denaturing TBE agarose gel electrophoresis.
517
518 **Electrophoretic mobility shift assay**
519 In a total volume of 20 µL 5 nM radioactively labeled RNA, 100 µg/mL yeast tRNA competitor,
520 and protein at a given concentration were mixed in buffer (20 mM Hepes, pH 7.8, 200 mM NaCl, 2 mM
521 $MgCl_2$, 2 mM DTT) with 4 % (v/v) glycerol. After 25 min at room temperature, the samples were resolved
522 by native TBE PAGE (6 % polyacrylamide) and gels incubated for 15 min in fixing solution (10 % (v/v)

523 acetic acid, 30 % (v/v) methanol) and subsequently vacuum dried. Gels were analyzed with radiograph
524 films or by a using Phosphorimager (FujifilmFLA5100).
525
526 **Surface plasmon resonance analysis (SPR)**
527 SPR experiments were performed with a BIACORE 3000 system (GE Healthcare). For protein-
528 RNA interactions, biotinylated RNA was streptavidin-captured on an SA-Chip (GE Healthcare) surface
529 according to manufacturers instructions. Measurements were performed at a flow rate of 30 µL/min in
530 standard buffer. Data were analyzed using the BIAevaluation software (GE Healthcare). Sample
531 sensograms were referenced against the signal in a ligand-free reference channel, and averaged values at
532 the equilibrium calculated. Steady state binding curves were obtained by plotting the response units at
533 equilibrium against protein concentration with the Origin Pro 9.0 (OriginLab) software.
534
535 **Computational quality check of the folds of the experimental constructs**
536 Part of the design of experimental constructs (minimal, config-switch) for the *in-vitro* and *in-vivo*
537 approaches was a quality check with *Kinefold*: The conformations of their sequences were predicted to
538 ensure that their expected conformation would be in agreement with the SRS consensus model
539
540 **Acknowledgements**
541 We would like to thank Herve Isambert for helpful discussions regarding Kinefold and Toby
542 Gibson for further support of M.S. This work was supported by the Deutsche Forschungs–gemeinschaft
543 (DFG, German Research Foundation) to R.-P.J. (DFG-FOR2333, Project Number 270067186), to M.F.
544 (CEPLAS EXC 1028, CRC1208, DFG-FOR2333, DFG Fe448/8, DFG Fe448/9), to D.N. (DFG-FOR2333,
545 Project Number 270067186), and to Z.K. (DFG-FOR2333, Project Number 270067186).
546
547 **Declaration of Interest**
548 The authors declare no potential conflicts of interest.

549 **References**

550 (1)Eliscovich, C.; Singer, R. H. RNP Transport in Cell Biology: The Long and Winding Road. *Curr.*
551 *Opin. Cell Biol.* **2017**, *45*, 38–46. https://doi.org/10.1016/j.ceb.2017.02.008.

552 (2)Bashirullah, A.; Cooperstock, R. L.; Lipshitz, H. D. RNA Localization in Development. *Annu. Rev.*
553 *Biochem.* **1998**, *67*, 335–394. https://doi.org/10.1146/annurev.biochem.67.1.335.

554 (3)Johnstone, O.; Lasko, P. Translational Regulation and RNA Localization in Drosophila Oocytes and
555 Embryos. *Annu. Rev. Genet.* **2001**, *35*, 365–406.
556 https://doi.org/10.1146/annurev.genet.35.102401.090756.

557 (4)Kloc, M.; Bilinski, S.; Chan, A. P.; Allen, L. H.; Zearfoss, N. R.; Etkin, L. D. RNA Localization and
558 Germ Cell Determination in Xenopus. *Int. Rev. Cytol.* **2001**, *203*, 63–91.
559 https://doi.org/10.1016/s0074-7696(01)03004-2.

560 (5)Palacios, I. M.; St Johnston, D. Getting the Message across: The Intracellular Localization of mRNAs
561 in Higher Eukaryotes. *Annu. Rev. Cell Dev. Biol.* **2001**, *17*, 569–614.
562 https://doi.org/10.1146/annurev.cellbio.17.1.569.

563 (6)Dahm, R.; Kiebler, M.; Macchi, P. RNA Localisation in the Nervous System. *Semin. Cell Dev. Biol.*
564 **2007**, *18* (2), 216–223. https://doi.org/10.1016/j.semcdb.2007.01.009.

565 (7)Abouward, R.; Schiavo, G. Walking the Line: Mechanisms Underlying Directional mRNA Transport
566 and Localisation in Neurons and Beyond. *Cell. Mol. Life Sci. CMLS* **2021**, *78* (6), 2665–2681.
567 https://doi.org/10.1007/s00018-020-03724-3.

568 (8)Edelmann, F. T.; Schlundt, A.; Heym, R. G.; Jenner, A.; Niedner-Boblenz, A.; Syed, M. I.; Paillart, J.-
569 C.; Stehle, R.; Janowski, R.; Sattler, M.; Jansen, R.-P.; Niessing, D. Molecular Architecture and
570 Dynamics of ASH1 mRNA Recognition by Its mRNA-Transport Complex. *Nat. Publ. Group* **2017**,
571 *24* (2), 152–161.

572 (9)Niedner, A.; Edelmann, F. T.; Niessing, D. Of Social Molecules: The Interactive Assembly of ASH1
573 mRNA-Transport Complexes in Yeast. *RNA Biol.* **2014**, *11* (8), 998–1009.
574 https://doi.org/10.4161/rna.29946.

575 (10) Olivier, C.; Poirier, G.; Gendron, P.; Boisgontier, A.; Major, F.; Chartrand, P. Identification of a
576 Conserved RNA Motif Essential for She2p Recognition and mRNA Localization to the Yeast Bud.
577 *Mol. Cell. Biol.* **2005**, *25* (11), 4752–4766. https://doi.org/10.1128/MCB.25.11.4752-4766.2005.
578 (11) Patel, V. L.; Mitra, S.; Harris, R.; Buxbaum, A. R.; Lionnet, T.; Brenowitz, M.; Girvin, M.; Levy,
579 M.; Almo, S. C.; Singer, R. H.; Chao, J. A. Spatial Arrangement of an RNA Zipcode Identifies
580 mRNAs under Post-Transcriptional Control. *Genes Dev.* **2012**, *26* (1), 43–53.
581 https://doi.org/10.1101/gad.177428.111.
582 (12) Chartrand, P.; Singer, R. H.; Long, R. M. RNP Localization and Transport in Yeast. *Annu. Rev. Cell*
583 *Dev. Biol.* **2001**, *17*, 297–310. https://doi.org/10.1146/annurev.cellbio.17.1.297.
584 (13) Chartrand, P.; Meng, X. H.; Singer, R. H.; Long, R. M. Structural Elements Required for the
585 Localization of ASH1 mRNA and of a Green Fluorescent Protein Reporter Particle in Vivo. *Curr.*
586 *Biol. CB* **1999**, *9* (6), 333–336. https://doi.org/10.1016/s0960-9822(99)80144-4.
587 (14) Gonzalez, I.; Buonomo, S. B. C.; Nasmyth, K.; von Ahsen, U. ASH1 mRNA Localization in Yeast
588 Involves Multiple Secondary Structural Elementsand Ash1 Protein Translation. *Curr. Biol. CB*
589 **1999**, *9* (6), 337–340.
590 (15) Kanke, M.; Jambor, H.; Reich, J.; Marches, B.; Gstir, R.; Ryu, Y. H.; Ephrussi, A.; Macdonald, P.
591 M. Oskar RNA Plays Multiple Noncoding Roles to Support Oogenesis and Maintain Integrity of the
592 Germline/Soma Distinction. *RNA N. Y. N* **2015**, *21* (6), 1096–1109.
593 https://doi.org/10.1261/rna.048298.114.
594 (16) Mori, Y.; Imaizumi, K.; Katayama, T.; Yoneda, T.; Tohyama, M. Two Cis-Acting Elements in the
595 3' Untranslated Region of Alpha-CaMKII Regulate Its Dendritic Targeting. *Nat. Neurosci.* **2000**, *3*
596 (11), 1079–1084. https://doi.org/10.1038/80591.
597 (17) Serano, J.; Rubin, G. M. The Drosophila Synaptotagmin-like Protein Bitesize Is Required for
598 Growth and Has mRNA Localization Sequences within Its Open Reading Frame. *Proc. Natl. Acad.*
599 *Sci. U. S. A.* **2003**, *100* (23), 13368–13373. https://doi.org/10.1073/pnas.1835727100.

600 (18) Thio, G. L.; Ray, R. P.; Barcelo, G.; Schüpbach, T. Localization of Gurken RNA in Drosophila
601 Oogenesis Requires Elements in the 5' and 3' Regions of the Transcript. *Dev. Biol.* **2000**, *221* (2),
602 435–446. https://doi.org/10.1006/dbio.2000.9690.
603 (19) Long, R. M.; Gu, W.; Lorimer, E.; Singer, R. H.; Chartrand, P. She2p Is a Novel RNA-Binding
604 Protein That Recruits the Myo4p-She3p Complex to ASH1 mRNA. *EMBO J.* **2000**, *19* (23), 6592–
605 6601. https://doi.org/10.1093/emboj/19.23.6592.
606 (20) Münchow, S.; Sauter, C.; Jansen, R. P. Association of the Class V Myosin Myo4p with a Localised
607 Messenger RNA in Budding Yeast Depends on She Proteins. *J. Cell Sci.* **1999**, *112 (Pt 10)*, 1511–
608 1518.
609 (21) Bertrand, E.; Chartrand, P.; Schaefer, M.; Shenoy, S. M.; Singer, R. H.; Long, R. M. Localization of
610 ASH1 mRNA Particles in Living Yeast. *Mol. Cell* **1998**, *2* (4), 437–445.
611 https://doi.org/10.1016/s1097-2765(00)80143-4.
612 (22) Böhl, F.; Kruse, C.; Frank, A.; Ferring, D.; Jansen, R. P. She2p, a Novel RNA-Binding Protein
613 Tethers ASH1 mRNA to the Myo4p Myosin Motor via She3p. *EMBO J.* **2000**, *19* (20), 5514–5524.
614 https://doi.org/10.1093/emboj/19.20.5514.
615 (23) Heym, R. G.; Zimmermann, D.; Edelmann, F. T.; Israel, L.; Ökten, Z.; Kovar, D. R.; Niessing, D. In
616 Vitro Reconstitution of an mRNA-Transport Complex Reveals Mechanisms of Assembly and Motor
617 Activation. *J. Cell Biol.* **2013**, *203* (6), 971–984. https://doi.org/10.1083/jcb.201302095.
618 (24) Takizawa, P. A.; Vale, R. D. The Myosin Motor, Myo4p, Binds Ash1 mRNA via the Adapter
619 Protein, She3p. *Proc. Natl. Acad. Sci.* **2000**, *97* (10), 5273–5278.
620 (25) Chartrand, P.; Meng, X. H.; Huttelmaier, S.; Donato, D.; Singer, R. H. Asymmetric Sorting of
621 Ash1p in Yeast Results from Inhibition of Translation by Localization Elements in the mRNA. *Mol.*
622 *Cell* **2002**, *10* (6), 1319–1330. https://doi.org/10.1016/s1097-2765(02)00694-9.
623 (26) Long, R. M.; Singer, R. H.; Meng, X.; Gonzalez, I.; Nasmyth, K.; Jansen, R. P. Mating Type
624 Switching in Yeast Controlled by Asymmetric Localization of ASH1 mRNA. *Science* **1997**, *277*
625 (5324), 383–387. https://doi.org/10.1126/science.277.5324.383.

626 (27) Sil, A.; Herskowitz, I. Identification of Asymmetrically Localized Determinant, Ash1p, Required
627 for Lineage-Specific Transcription of the Yeast HO Gene. *Cell* **1996**, *84* (5), 711–722.
628 https://doi.org/10.1016/s0092-8674(00)81049-1.
629 (28) Takizawa, P. A.; Sil, A.; Swedlow, J. R.; Herskowitz, I.; Vale, R. D. Actin-Dependent Localization
630 of an RNA Encoding a Cell-Fate Determinant in Yeast. *Nature* **1997**, *389* (6646), 90–93.
631 https://doi.org/10.1038/38015.
632 (29) Shepard, K. A.; Gerber, A. P.; Jambhekar, A.; Takizawa, P. A.; Brown, P. O.; Herschlag, D.;
633 DeRisi, J. L.; Vale, R. D. Widespread Cytoplasmic mRNA Transport in Yeast: Identification of 22
634 Bud-Localized Transcripts Using DNA Microarray Analysis. *Proc. Natl. Acad. Sci. U. S. A.* **2003**,
635 *100* (20), 11429–11434. https://doi.org/10.1073/pnas.2033246100.
636 (30) Jambhekar, A.; McDermott, K.; Sorber, K.; Shepard, K. A.; Vale, R. D.; Takizawa, P. A.; DeRisi, J.
637 L. Unbiased Selection of Localization Elements Reveals Cis-Acting Determinants of mRNA Bud
638 Localization in Saccharomyces Cerevisiae. *Proc. Natl. Acad. Sci. U. S. A.* **2005**, *102* (50), 18005–
639 18010. https://doi.org/10.1073/pnas.0509229102.
640 (31) Singh, N.; Blobel, G.; Shi, H. Hooking She3p onto She2p for Myosin-Mediated Cytoplasmic
641 mRNA Transport. *Proc. Natl. Acad. Sci. U. S. A.* **2015**, *112* (1), 142–147.
642 https://doi.org/10.1073/pnas.1423194112.
643 (32) Xayaphoummine, A.; Bucher, T.; Isambert, H. Kinefold Web Server for RNA/DNA Folding Path
644 and Structure Prediction Including Pseudoknots and Knots. *Nucleic Acids Res.* **2005**, *33* (Web
645 Server issue), W605-610. https://doi.org/10.1093/nar/gki447.
646 (33) Kertesz, M.; Wan, Y.; Mazor, E.; Rinn, J. L.; Nutter, R. C.; Chang, H. Y.; Segal, E. Genome-Wide
647 Measurement of RNA Secondary Structure in Yeast. *Nature* **2010**, *467* (7311), 103–107.
648 https://doi.org/10.1038/nature09322.
649 (34) Tutucci, E.; Maekiniemi, A.; Snoep, J. L.; Seiler, M.; van Rossum, K.; van Niekerk, D. D.; Savakis,
650 P.; Zarnack, K.; Singer, R. H. *Cyclin CLB2 mRNA Localization Determines Efficient Protein*

651 *Synthesis to Orchestrate Bud Growth and Cell Cycle Progression*; preprint; Cell Biology, 2022.
652 https://doi.org/10.1101/2022.03.01.481833.
653 (35) Frankel, A. D. If the Loop Fits. *Nat. Struct. Biol.* **1999**, *6* (12), 1081–1083.
654 https://doi.org/10.1038/70002.
655 (36) Takizawa, P. A.; DeRisi, J. L.; Wilhelm, J. E.; Vale, R. D. Plasma Membrane Compartmentalization
656 in Yeast by Messenger RNA Transport and a Septin Diffusion Barrier. *Science* **2000**, *290* (5490),
657 341–344. https://doi.org/10.1126/science.290.5490.341.
658 (37) Müller, M.; Richter, K.; Heuck, A.; Kremmer, E.; Buchner, J.; Jansen, R.-P.; Niessing, D.
659 Formation of She2p Tetramers Is Required for mRNA Binding, mRNP Assembly, and Localization.
660 *RNA N. Y. N* **2009**, *15* (11), 2002–2012.
661 (38) Lorenz, R.; Bernhart, S. H.; Höner Zu Siederdissen, C.; Tafer, H.; Flamm, C.; Stadler, P. F.;
662 Hofacker, I. L. ViennaRNA Package 2.0. *Algorithms Mol. Biol. AMB* **2011**, *6*, 26.
663 https://doi.org/10.1186/1748-7188-6-26.
664 (39) Reuter, J. S.; Mathews, D. H. RNAstructure: Software for RNA Secondary Structure Prediction and
665 Analysis. *BMC Bioinformatics* **2010**, *11*, 129. https://doi.org/10.1186/1471-2105-11-129.
666 (40) Zuker, M. Mfold Web Server for Nucleic Acid Folding and Hybridization Prediction. *Nucleic Acids*
667 *Res.* **2003**, *31* (13), 3406–3415. https://doi.org/10.1093/nar/gkg595.
668 (41) Seiler, M.; Mehrle, A.; Poustka, A.; Wiemann, S. The 3of5 Web Application for Complex and
669 Comprehensive Pattern Matching in Protein Sequences. *BMC Bioinformatics* **2006**, *7*, 144.
670 https://doi.org/10.1186/1471-2105-7-144.
671 (42) Schrödinger, L.; DeLano, W. PyMOL. **2020**.
672 (43) Kumar, M.; Michael, S.; Alvarado-Valverde, J.; Mészáros, B.; Sámano-Sánchez, H.; Zeke, A.;
673 Dobson, L.; Lazar, T.; Örd, M.; Nagpal, A.; Farahi, N.; Käser, M.; Kraleti, R.; Davey, N. E.;
674 Pancsa, R.; Chemes, L. B.; Gibson, T. J. The Eukaryotic Linear Motif Resource: 2022 Release.
675 *Nucleic Acids Res.* **2022**, *50* (D1), D497–D508. https://doi.org/10.1093/nar/gkab975.

(44) Waterhouse, A. M.; Procter, J. B.; Martin, D. M. A.; Clamp, M.; Barton, G. J. Jalview Version 2--a Multiple Sequence Alignment Editor and Analysis Workbench. *Bioinforma. Oxf. Engl.* **2009**, *25* (9), 1189–1191. https://doi.org/10.1093/bioinformatics/btp033.

(45) Engel, S. R.; Dietrich, F. S.; Fisk, D. G.; Binkley, G.; Balakrishnan, R.; Costanzo, M. C.; Dwight, S. S.; Hitz, B. C.; Karra, K.; Nash, R. S.; Weng, S.; Wong, E. D.; Lloyd, P.; Skrzypek, M. S.; Miyasato, S. R.; Simison, M.; Cherry, J. M. The Reference Genome Sequence of Saccharomyces Cerevisiae: Then and Now. *G3 Bethesda Md* **2014**, *4* (3), 389–398. https://doi.org/10.1534/g3.113.008995.

(46) Engel, S. R.; Wong, E. D.; Nash, R. S.; Aleksander, S.; Alexander, M.; Douglass, E.; Karra, K.; Miyasato, S. R.; Simison, M.; Skrzypek, M. S.; Weng, S.; Cherry, J. M. New Data and Collaborations at the Saccharomyces Genome Database: Updated Reference Genome, Alleles, and the Alliance of Genome Resources. *Genetics* **2022**, *220* (4), iyab224. https://doi.org/10.1093/genetics/iyab224.

(47) Darty, K.; Denise, A.; Ponty, Y. VARNA: Interactive Drawing and Editing of the RNA Secondary Structure. *Bioinforma. Oxf. Engl.* **2009**, *25* (15), 1974–1975. https://doi.org/10.1093/bioinformatics/btp250.

696 **Figures Legends**

697 **Figure 1. The SRS consensus model describes all four *ASH1* SRS elements. A** Left, conformational
698 prediction of $E3_{1771-1821}$ by Kinefold displays the asymmetric bulge as a strand of 5 nt ('Lbulge') juxtaposed
699 with a shorter strand ('Sbulge')(both marked in red). Functionally relevant cytosines are boxed in green.
700 The asymmetric bulge and the lengths of Lbulge and Sbulge are marked in red, previously known functional
701 motifs in dark green. Right, the conformation of E3 referred to its crystal structure bound to She2p/3p
702 (**PDB: 5NEW**) displayed an rearrangement of the asymmetric bulge, in a ratio (Lbulge/Sbulge of
703 6:3)(uncommon base-pairs ignored in counting but dashed in blue), with sequence motifs adapted to
704 analogous positions in E2A, E2B and E3 (light green). **B** Left, Kinefold prediction and 180° rotation of
705 $E2A_{1109-1185}$ revealed an asymmetric bulge with the same 5:2 ratio as in E3. Right, the high degree of
706 sequence similarity (**Supplementary Fig. 1**) enabled a modeling in tight accordance to the E3 conformation
707 of the crystal structure that even comprised the uncommon base-pairing C_{1122}-C_{1174} and the A_{1123}-A_{1169} base-
708 stacking (dashed in blue). **C** Left, the predicted conformation of $E2B_{1263-1320}$ after 180°rotation showed
709 internal repeats (left, boxed in orange) that had to be aligned to adapt the consensus conformation (right)
710 that Kinefold also predicted but with 28% gain of energy content (-10.3 kcal/mol vs.-7.4 kcal/mol). **D** SRS
711 element $E2B_{623-701}$ after Kinefold prediction and 180°rotation (left) and after adaption (right). **E** Scheme of
712 the common features of all four modeled SRS elements, projected on $E3_{1771-1821}$. An asymmetric bulge(red)
713 is framed by two inverted repeats (yellow), with sequence motifs indicated in green. **F** Schematic
714 presentation of the SRS consensus model with its features displayed in the two configurations (IR1 boxed
715 in grey, IR2 boxed in blue, Lbulge and Sbulge in red, sequence motifs in green). The SRS consensus model
716 is characterized by a conformational feature arrangement that is identical in both configurations (middle),
717 but with differing linear order of features at sequence level (left). As a result, the positioning of sequence
718 start and end differ between the configurations in the conformational view (middle). Right, derived scheme
719 of the SRS consensus model that unifies the conformational arrangement of both configurations.
720

721 **Figure 2. The modeling of the SRS consensus involves choice of appropriate conformation prediction**
722 **tool, rotation and mutual feature alignment of the four SRS elements in *ASH1*.** The overview
723 demonstrates the effects of the three steps of modeling on the extended sizes of the *ASH1* SRS elements as
724 they were characterized before. Whereas the initially known conformations displayed a huge degree of
725 heterogeneity (**A, D, H, L**), the conformation prediction tool Kinefold tolerated asymmetric bulges in each
726 SRS element (**B, E, I, M**). For E3, using the published crystal structure as a blue print, its conformational
727 prediction (**B**) was adapted, with altered conformation of the asymmetric bulge (resulting in atypical base
728 pairings, marked in red, **C**). Its final asymmetric feature is indicated by a red triangle, with the numbers of

729 nucleotides displayed for both, Lbulge and Sbulge. By later analyses, we could assign one of its functional
730 cytosines as being analogous to already known CGA sequence motifs with other SRS elements (indicated
731 in red). For E2A, E1 and E2B, it was the rotation of the initial predictions that harmonized the respective
732 conformations with E3 (**F, J, N**). For E2A, due to its remarkable sequence identity with E3, we could also
733 introduce the same atypical base pairings (marked in red, **G**). As mentioned before, E2B represented an
734 outlier: it was a alternative conformation prediction that could be harmonized with E3, suggesting the need
735 of a further intramolecular rearrangement to align the inverted boxes (marked in yellow, **N** vs. **O**).
736
737 **Figure 3. The configuration switch in E3 displays conserved function and surface plasmon resonance**
738 **analysis confirms the optimal C_1-C_2 distance of 6 nt in minimal constructs of E3. A** Representative
739 results of electrophoretic mobility shift assays (EMSA) of triplicates to analyze complex formation of wild-
740 type and variant constructs of radioactive ASH1 $E3_{51nt}$ RNA with the She2p-She3p fusion protein ($She2p_{6-}$
741 $_{246}$-$(GGSGG)_2$-$She3p_{331-405}$) in increasing concentration (0.02 - 5 μM): Wildtype $E3_{1771-1821}$ (left), construct
742 with switch of $E3_{1771-1821}$ from config-I to config-II (middle) and control M6 mutational variant of $E3_{1771-}$
743 $_{1821}$ with decreased SRS function [8]. **B** Results of surface plasmon resonance analysis (SRP), performed in
744 triplicates to analyze the minimal E3 constructs and alterations in their C_1-C_2 distance. The minimal
745 construct $E3_{28nt}$wt was re-designed to create constructs with differing C1-C2 distances (5 and 7 nt) and was
746 incubated with She2p-She3p fusion protein (125 nM).
747
748 **Figure 4. Computational screen for the SRS consensus model across 24 known She2p/3p interactors**
749 **results in 31 predictions of both configurations in 17 sequences. A** Computational prediction of SRS
750 instances by feature screening of the SRS consensus model and evaluation of the resulting, predicted RNA
751 conformations (**Materials and Methods**). The screen was applied on 24 sequences for She2p/3p interaction
752 with varying experimental confidence (**Supplementary Tab. 1**). It identified 31 SRS predictions in 17
753 sequences, visualized as bar charts, with their coding sequences (rectangles) and 3' UTR extensions (200
754 nt, black lines). SRS predictions were indicated by their configurations (config-I: red, config-II: blue). **B**
755 For the SRS predictions of each configuration, the number of occurrences of the AA_L dinucleotide was
756 specified. **C** Schematic overview on the high-confidential set of SRS elements. Similar to the SRS elements
757 in *ASH1*, predictions in *IST2*, *EAR1* and *WSC2* matched published, well-characterized SRS elements (SRS
758 nomenclature, see *SRS collection*, **Tab. 2**) and could be arranged in the scheme of the SRS consensus model.
759 Color scheme is according to **Figure 1**, with further visualization of AA_L dinucleotides in the Lbulge and
760 adjacent regions, boxed in orange). Uncommon base pairings had been shown for the E3-She2p/She3p
761 crystal structure and were mapped on E2A that displayed high sequence similarity with E3 after rotation
762 (blue-dashed). Of note, similar uncommon base-pairings may also arise in E1 and *IST2*-SRS-2.

763

764 **Figure 5. The configuration switch in the minimal SRS constructs of *EAR*-SRS2, *IST*-SRS2, *KSS1*-**
765 **SRS1 and *TCB3*-SRS1 displays conserved SRS function in electrophoretic mobility shift assays.**
766 Representative results of electrophoretic mobility shift assays (EMSA) to analyze interaction of radioactive
767 wild-type and designed RNA constructs with the She2p-She3p fusion protein (She2p$_{6\text{-}246}$-(GGSGG)$_2$-
768 She3p$_{331\text{-}405}$) in increasing concentration (0.02 - 5 μM). All minimal constructs were designed switched in
769 configuration (from config-II to config-I). Their final loop sequence GAAA referred to the artificial loop
770 sequence of the E3 constructs in [8] that was shown not to modify SRS function. **A** EMSA experiments of
771 well-known SRS elements. Left, *EAR1*-SRS2$_{1572\text{-}1621}$ (config-II) was studied as wildtype construct *EAR1*-
772 SRS2$_{50nt}$wt and as config-switched, minimal construct *EAR1*-SRS2$_{26nt\text{-}}$switch (config-I). Right, *IST2*-
773 SRS2$_{2716\text{-}2777}$ (config-II) was studied as wildtype construct *IST2*-SRS2$_{62nt}$wt and as config-switched,
774 minimal construct *IST2*-SRS2$_{29nt\text{-}}$switch (config-I). **B** EMSA experiments of new, predicted SRS elements.
775 Left, *KSS1*-SRS1 (config-II) was studied as wildtype construct *KSS1*-SRS1$_{72nt}$wt and as config-switched,
776 minimal construct *KSS1*-SRS1$_{29nt\text{-}}$switch (config-I). Right, *TCB3*-SRS1 (config-II) was studied as config-
777 switched, minimal construct *TCB3*-SRS1$_{38nt\text{-}}$switch (config-I).
778

779 **Figure 6 *EAR1*-SRS2 is partly sensitive to alterations of its functional motifs but tolerates alterations**
780 **in its conformational features and in the AA$_L$ dinucleotide of the Lbulge as confirmed for its minimal,**
781 **config-switched construct by surface plasmon resonance analysis. A** Schemes of the minimal constructs
782 of *EAR1*-SRS2$_{28nt}$switch that were re-designed to create constructs with altered conformational features
783 (indicated in red in conformations). The final loop sequence GAAA referred to the artificial loop sequence
784 of the E3 constructs in [8] that was shown not to modify SRS function **B** Substitution scheme to analyze the
785 relevance of cytosines in the sequence motifs of the SRS consensus model. Alterations are marked in red
786 in substitution tables that refer to both, sequence positions and terminologies of resulting constructs. Since
787 two cytosines (C_{1601} and C_{1602}) precluded an unambiguous assignment of the C_1 position, both had to be
788 considered. A third cytosine C_{1600}, marked by a star, was not considered in alterations due to its
789 uncommonly short distance to C_2. **C** Substitution scheme to analyze the relevance of the AA$_L$ dinucleotide
790 in the Lbulge. For each alterations, construct name (blue), conserved sequence in the Lbulge (black) and
791 alterations (red) are displayed. **D** Results of surface plasmon resonance analysis (SRP), performed in
792 triplicates to analyze the minimal EAR1-SRS2 constructs and alterations in their C_1-C_2 distance. E3 RNA
793 was incubated with She2p-She3p fusion protein (125 nM).
794
795

Figure 1

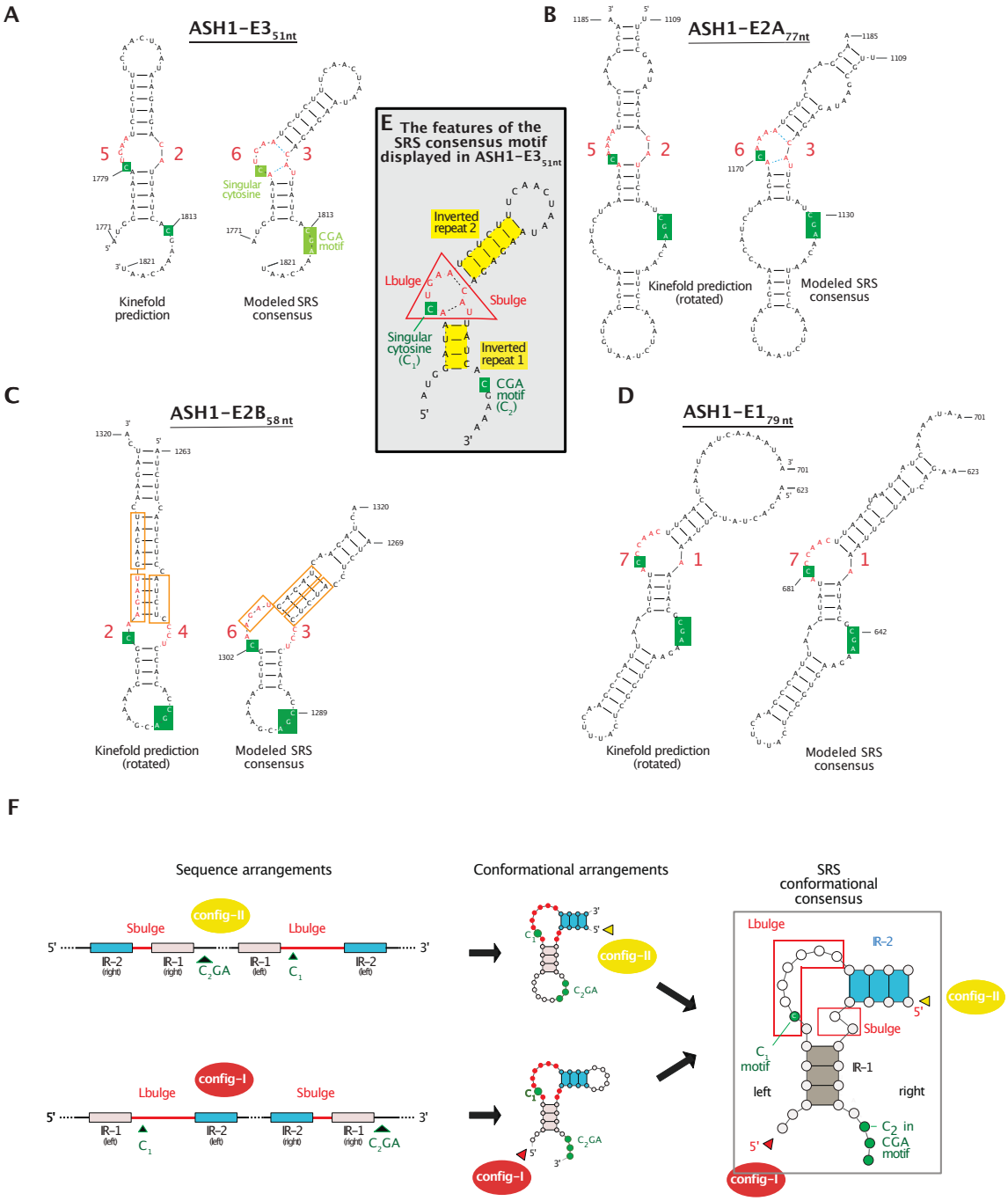
A
ASH1-E3 51nt
Kinefold prediction
Modeled SRS consensus
Singular cytosine
CGA motif
B
ASH1-E2A 77nt
Kinefold prediction (rotated)
Modeled SRS consensus
E The features of the SRS consensus motif displayed in ASH1-E3 51nt
Inverted repeat 2
Lbulge
Sbulge
Singular cytosine (C1)
Inverted repeat 1
CGA motif (C2)
C
ASH1-E2B 58 nt
Kinefold prediction (rotated)
Modeled SRS consensus
D
ASH1-E1 79 nt
Kinefold prediction (rotated)
Modeled SRS consensus
F
Sequence arrangements
Conformational arrangements
SRS conformational consensus
config-II
config-I
Sbulge
Lbulge
IR-2
IR-1
C2GA
C1
C1 motif
left
right
C2 in CGA motif

Figure 2

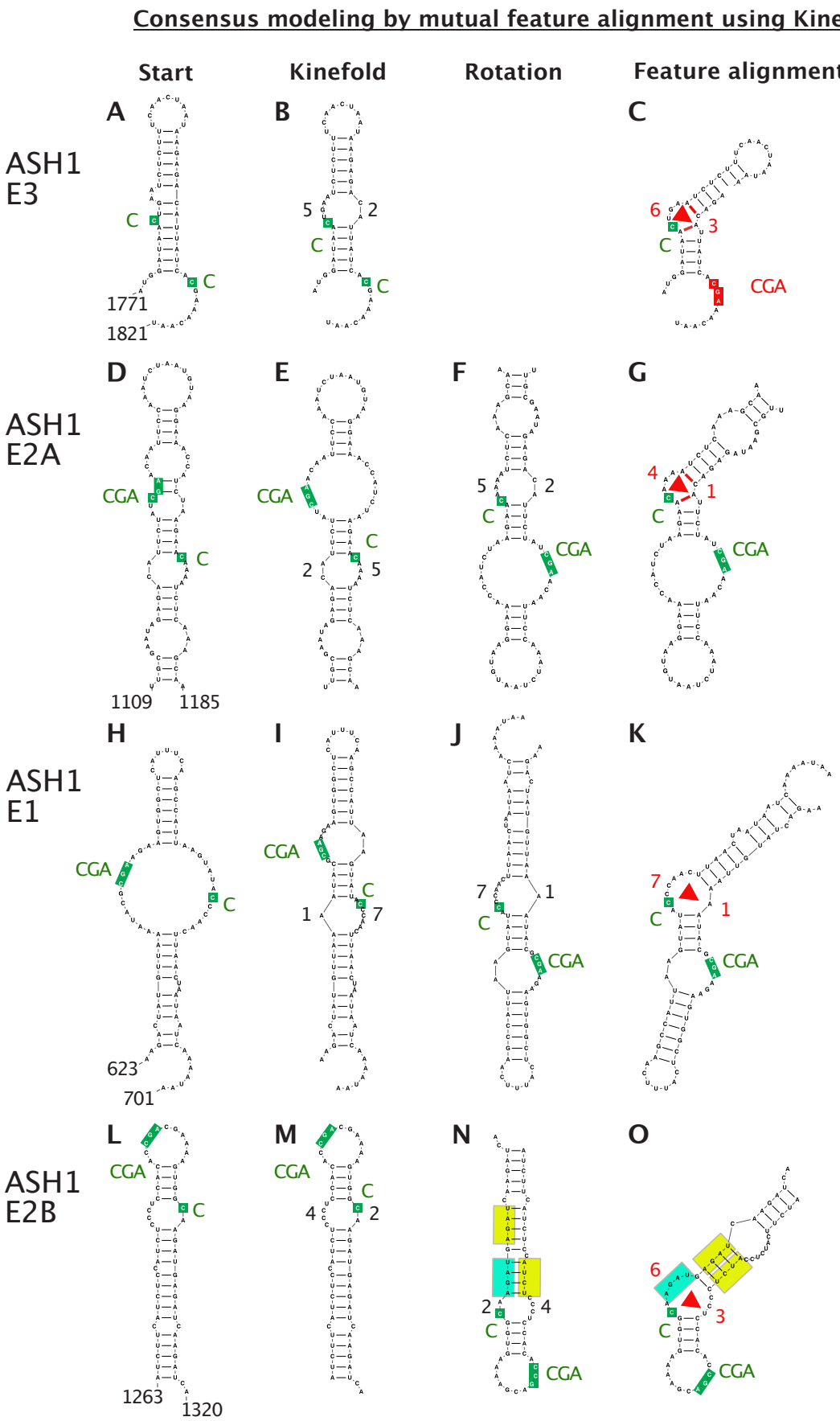
Consensus modeling by mutual feature alignment using Kinefold
Start
Kinefold
Rotation
Feature alignment
ASH1 E3
ASH1 E2A
ASH1 E1
ASH1 E2B
A
B
C
D
E
F
G
H
I
J
K
L
M
N
O
CGA
C
1771
1821
1109
1185
623
701
1263
1320

Figure 3

A

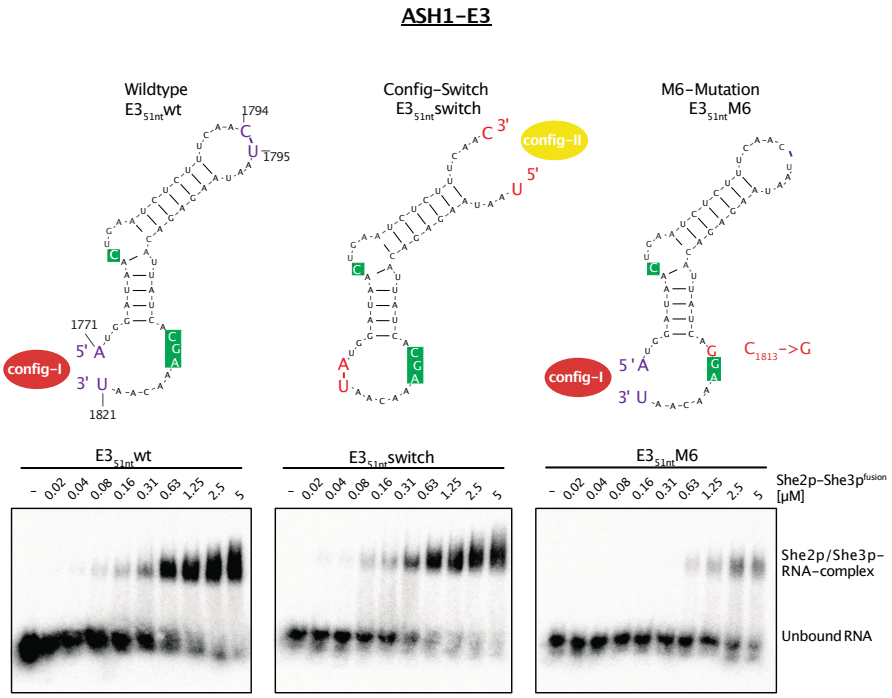
ASH1-E3
Wildtype
E3 51nt wt
1794
1795
1771
1821
5' A
3' U
config-I
Config-Switch
E3 51nt switch
C 3'
U 5'
config-II
A
U
M6-Mutation
E3 51nt M6
C1813->G
5' A
3' U
config-I
E3 51nt wt
E3 51nt switch
E3 51nt M6
- 0.02 0.04 0.08 0.16 0.31 0.63 1.25 2.5 5
She2p-She3p fusion [µM]
She2p/She3p-RNA-complex
Unbound RNA

B

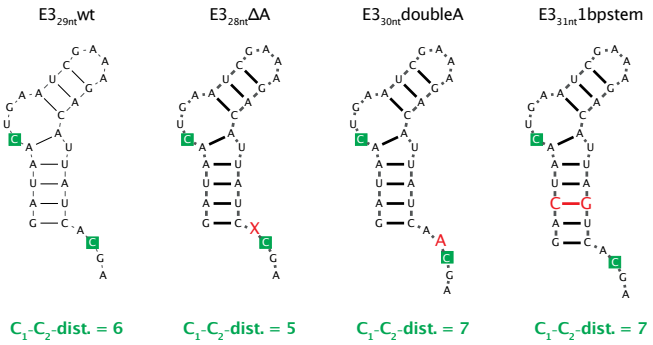
E3 29nt wt
E3 28nt ΔA
E3 30nt doubleA
E3 31nt 1bpstem
C1-C2-dist. = 6
C1-C2-dist. = 5
C1-C2-dist. = 7
C1-C2-dist. = 7

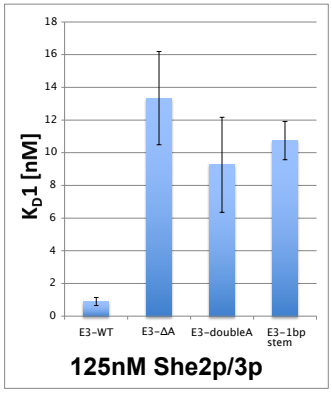
K D 1 [nM]
0
2
4
6
8
10
12
14
16
18
E3-WT
E3-ΔA
E3-doubleA
E3-1bp stem
125nM She2p/3p

Figure 4

A

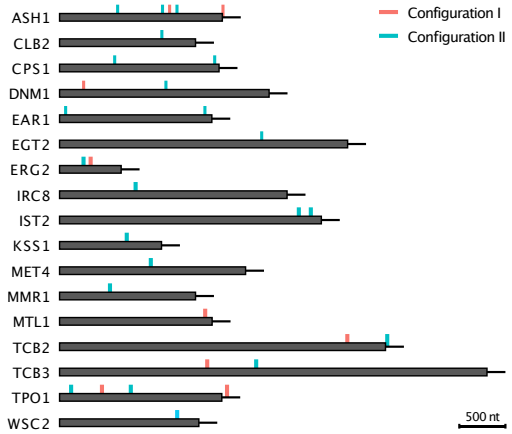
ASH1
CLB2
CPS1
DNM1
EAR1
EGT2
ERG2
IRC8
IST2
KSS1
MET4
MMR1
MTL1
TCB2
TCB3
TPO1
WSC2
Configuration I
Configuration II
500 nt

B

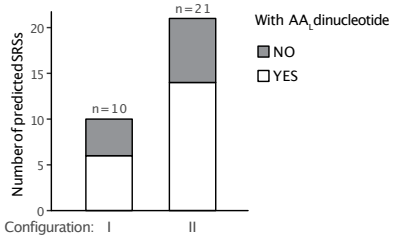
Number of predicted SRSs
0
5
10
15
20
n = 10
n = 21
Configuration: I
II
With AA$_L$ dinucleotide
NO
YES

C

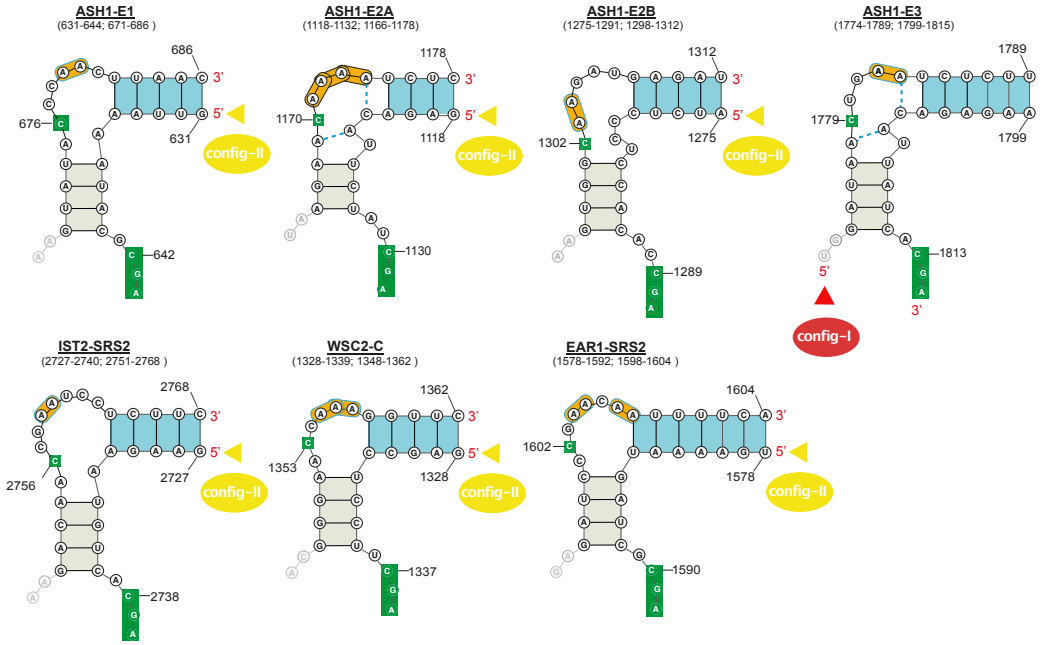
ASH1-E1
(631-644; 671-686)
686
676
631
642
3'
5'
config-II
ASH1-E2A
(1118-1132; 1166-1178)
1178
1170
1118
1130
ASH1-E2B
(1275-1291; 1298-1312)
1312
1302
1275
1289
ASH1-E3
(1774-1789; 1799-1815)
1789
1779
1799
1813
config-I
IST2-SRS2
(2727-2740; 2751-2768)
2768
2756
2727
2738
WSC2-C
(1328-1339; 1348-1362)
1362
1353
1328
1337
EAR1-SRS2
(1578-1592; 1598-1604)
1604
1602
1578
1590

Figure 5

A

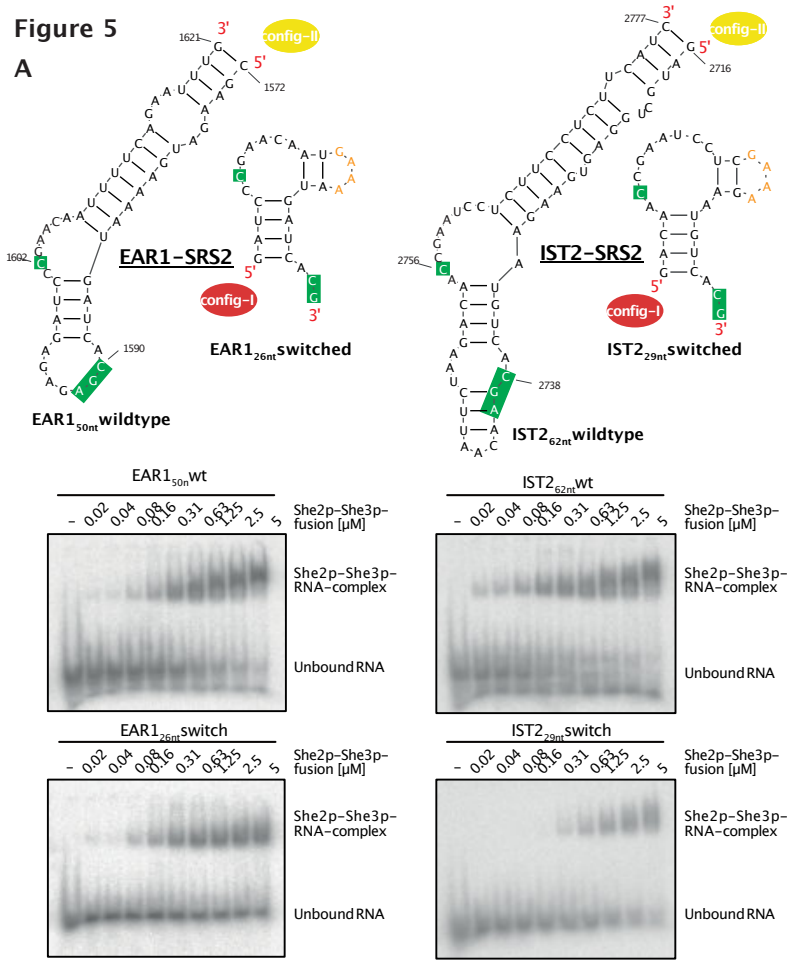
EAR1-SRS2
IST2-SRS2
config-II
config-I
EAR1$_{26nt}$switched
IST2$_{29nt}$switched
EAR1$_{50nt}$wildtype
IST2$_{62nt}$wildtype
EAR1$_{50n}$wt
IST2$_{62nt}$wt
EAR1$_{26nt}$switch
IST2$_{29nt}$switch
- 0.02 0.04 0.08 0.16 0.31 0.63 1.25 2.5 5
She2p-She3p-fusion [µM]
She2p-She3p-RNA-complex
Unbound RNA

B

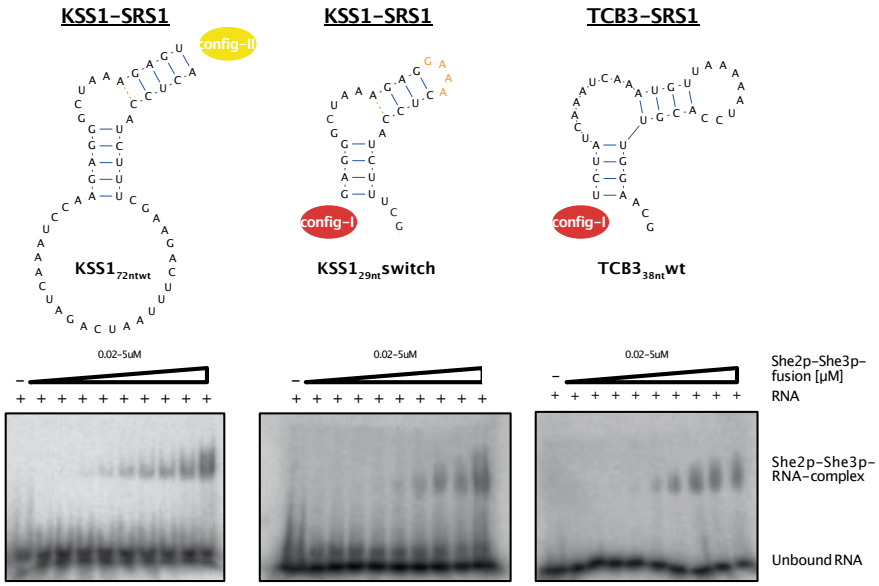
KSS1-SRS1
KSS1-SRS1
TCB3-SRS1
config-II
config-I
KSS1$_{72ntwt}$
KSS1$_{29nt}$switch
TCB3$_{38nt}$wt
0.02-5uM
She2p-She3p-fusion [µM]
RNA
She2p-She3p-RNA-complex
Unbound RNA

Figure 6

EAR1-SRS2 constructs for SRP analysis

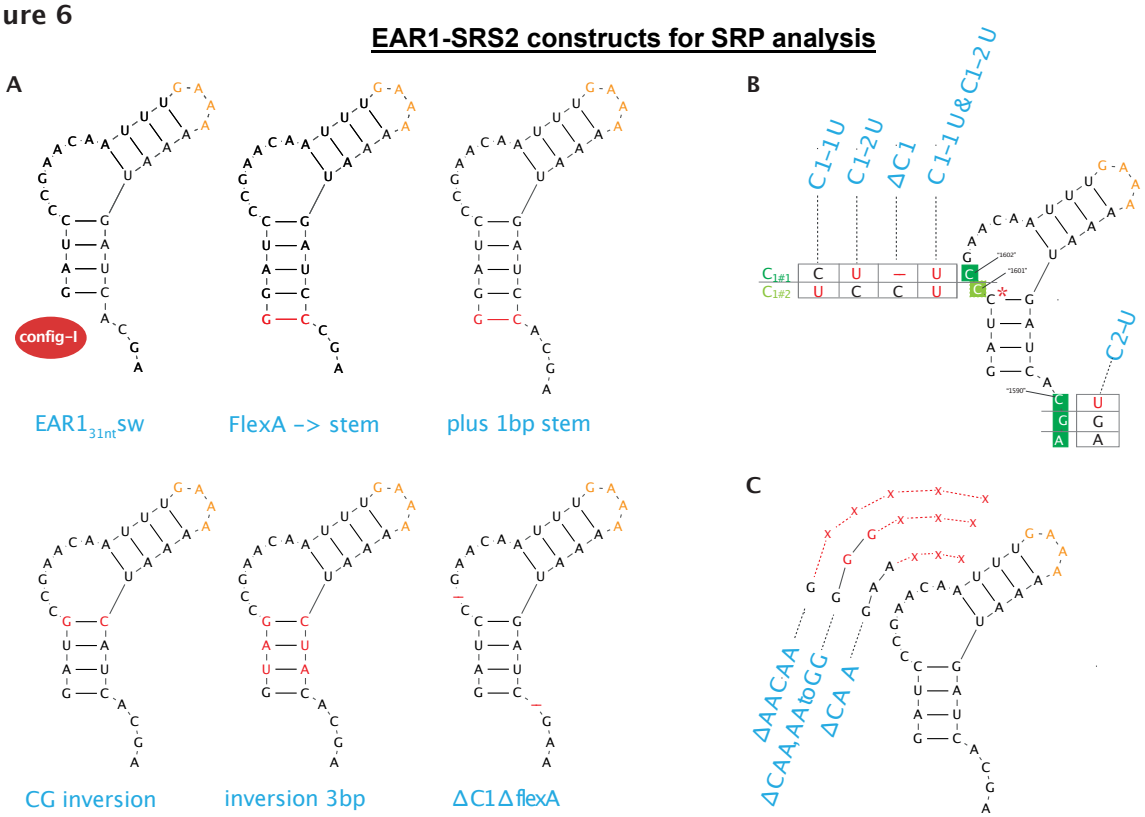

D

SRP: EAR1-SRS2 constructs vs. 125nM She2p/3p

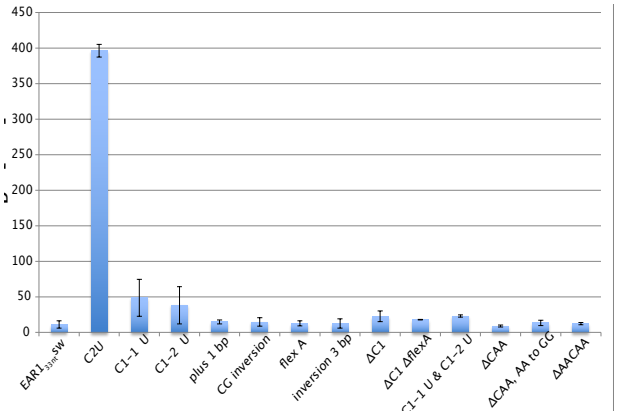

INFO-BOX: Summary of the SRS consensus motif

1. Two **inverted repeats** (IR-1, IR-2) flank an **asymmetric bulge** (consisting of **Lbulge** and **Sbulge**)
2. The conserved **singular cytosine C_1** resides in one of the first three positions of the Lbulge
3. The conserved **C_2GA triplet** resides in a further bulge, at the opposite strand of C_1, separated by an inverted repeat in downstream direction on this strand in a **C_1-C_2 distance of six positions**
4. The two **configurations** are marked by the two different 5' entry sites into the kinked SRS element conformation.

TABLE 1 Overview on the four localization elements of *ASH1*. Positions and configuration classification are listed according to the SRS consensus motif

SRS name	SRS config I	SRS config II	SRS AA motif in Lbulge	SRS start	SRS end
E2		II	yes	631	686
E2A		II	yes	1118	1178
E2B		II	yes	1275	1312
E3	I		yes	1774	1817

TABLE 2 Overview on the *SRS instance collection.* The columns list info at transcripts and SRS instance level; SRS instance are classified according to the SRS consensus motif (including positions and configuration); the last two columns contain information to the identification of SRS elements in fragment size or as a detailed description in previous publications and this study

mRNA #	mRNA name	mRNA gene ID	SRS instance also known as	SRS instance collection name (*)	SRS start	SRS end	SRS config I	SRS config II	SRS as terminal element (***)	SRS with AA motif	SRS fragment reference	SRS element reference
1	*ASH1*	*YKL185W*	E1	ASH1-E1	631	686		II		AA	several	several
			E2A	ASH1-E2A	1118	1178		II		AA	several	several
			E2B	ASH1-E2B	1275	1312		II	terminal	AA	several	several
			E3, U_{min}	ASH1-E3	1774	1817	I			AA	several	several
2	*CLB2*	*YPR119W*		CLB2-SRS1	1111	1145		II		AA		Tutucci et al
3	*CPS1*	*YJL172W*		CPS1-SRS1	599	636		II		AA		
				CPS1-SRS2	1684	1738		II		AA		
4	*DNM1*	*YLL001W*		DBM1-SRS1	262	302	I					
				DBM1-SRS2	1155	1189		II				
5	*EAR1*	*YMR171C*		EAR1-SRS1	110	167		II		AA		
				EAR1-SRS2	1578	1614		II	terminal	AA	Olivier et al	Olivier et al this study
6	*EGT2*	*YNL327W*		EGT2-SRS1	2194	2235		II		AA		
7	*ERG2*	*YMR202W*		ERG2-SRS1	261	314		II				
				ERG2-SRS2	338	380	I			AA		
8	*IRC8*	*YJL051W*		IRC8-SRS1	826	870		II		AA		
9	*IST2*	*YBR086C*		IST2-SRS1	2597	2626		II		AA		
				IST2-SRS2	2727	2768		II	terminal	AA	Olivier et al	Olivier et al this study
10	*KSS1*	*YGR040W*		KSS1-SRS1	730	781		II		AA		this study
11	*MET4*	*YNL103W*		MET4-SRS1	991	1051		II				
12	*MMR1*	*YLR190W*		MMR1-SRS1	548	590		II				
13	*MTL1*	*YGR023W*		MTL1-SRS1	1581	1651	I					
14	*TCB2*	*YNL087W*		TCB2-SRS1	3123	3175	I			AA		
				TCB2-SRS2	3556	3592		II		AA		
15	*TCB3*	*YML072C*		TCB3-SRS1	1603	1642	I			AA		this study
				TCB3-SRS2	2134	2173		II		AA		
16	*TPO1*	*YLL028W*		TPO1-SRS1	175	240		II		AA		
				TPO1-SRS2	461	527	I					
				TPO1-SRS3	774	822		II				
				TPO1-SRS4	1818	1862	I					
17	*WSC2*	*YNL283C*	WSC2N	WSC2-N	1277	1327	I			AA		Jambhekar et al
			WSC2C	WSC2-C	1326	1373		II		AA		Jambhekar et al

Remarks

SRS instances studies in this work are indicated in **red**.

(*) SRS names in SRS collection — previously existing SRS terminologies are kept
in case of non-existing previous terminologies, the nomenclature contains "-SRS" suffixes (**)

(**) Numbering with suffixes — the numbering follows their positions in 5'-3' RNA sequence.
SRS elements that were discovered later, are numbered with subsequent numbers

(***) SRS as terminal element — indicates such SRS instances that reside at the terminal region of a RNA stem fold